Nuclear Radii from Inelastic Cross-Section Measurements*

G. P. MILLBURN, W. BIRNBAUM,† W. E. CRANDALL,† AND L. SCHECTER†
Radiation Laboratory, Department of Physics, University of California, Berkeley, California
(Received April 9, 1954)

Inelastic cross sections for high-energy protons, deuterons, He^3 particles, and alpha particles accelerated in the 184-inch cyclotron were measured by an attenuation technique. All the cross sections vary as the square of the nuclear radius and indicate that if the nucleus has a fringe it increases as $A^{\frac{1}{3}}$. The derived value of the nuclear radius constant a_0 depends on the nuclear model and the particular bombarding particle. The effect of the nucleus is found to extend at least to a radius given by $a_0=(1.68\pm0.04)\times10^{-13}$ cm. Deuteron stripping cross sections were derived and found to vary approximately as the square root of the mass number.

I. INTRODUCTION

THE total inelastic cross sections of high-energy charged particles for several elements have been determined by an attenuation technique. Much of the emphasis in this report has been concentrated on the behavior of 190-Mev deuterons while traversing an absorbing medium, but the experimental technique has been extended to include the attenuation of 340-Mev protons, 490-Mev He^3 particles, and 380-Mev alpha particles. The latter cross sections have been determined with somewhat less precision because of the limitations of the experimental method and the consequent uncertainties in the interpretation of the data.

These attenuation cross sections are fundamental in the general understanding of nuclear processes. A comparison of the respective inelastic cross sections gives further information regarding the structure of the nucleus and the effects of nuclear transparency.[1] Furthermore, from the deuteron data, stripping cross sections[2] can be determined for the different elements serving as attenuators.

A summary of the high-energy neutron inelastic cross sections,[3–6] as well as the proton attenuation cross sections of Kirschbaum and Hicks,[7] and Chen *et al.*,[8] are presented together with the results of this experiment.

II. THEORY OF THE EXPERIMENTAL METHOD

A. Definition of Symbols

The following symbols will be used throughout the paper:

σ_{1p} = an effective attenuation cross section for protons.
σ_2 = the total inelastic or attenuation cross section for deuterons.
σ_3 = the total inelastic cross section for He^3 particles.
σ_4 = the total inelastic cross section for He^4 (alpha) particles.
σ_{2sp} = the cross section for the production of stripped protons from incident deuterons ($\sigma_{2sp}=\sigma_2-\sigma_{1p}$).
σ_{3sp} = the cross section for the production of one stripped proton from an incident He^3 particle [$\sigma_{3sp}=2(\sigma_3-\sigma_{1p})$].
R_1 = range of protons.
R_2 = range of deuterons.
R_{3He} = range of He^3.
R_4 = range of alpha particles.
r = nuclear radius, assumed to be given by $r=a_0A^{\frac{1}{3}}$.
t = absorber thickness.

B. Definition of an Inelastic Event

The definition of an inelastic event in this experiment is based upon range measurements. A particle is said to have suffered an inelastic collision if its range in the absorbing medium is shortened by a measurable amount. For the energies involved, the range-energy relation is approximately $R=\text{const}T^{1.8}$.[9] Therefore, the relative energy loss is given by $(\Delta T/T)=(1/1.8)\times(\Delta R/R)$. For 190-Mev deuterons, a change of range of 4 percent is easily detected: a deuteron event is considered inelastic only if the energy loss is 4 Mev or greater. In any case, because of its low binding energy, any inelastic collision will probably cause the deuteron to split up into its component nucleons. For 340-Mev protons, 490-Mev He^3 particles, and 380-Mev alpha particles, inelastic events are defined as those in which energy losses occur which are greater than 15 Mev.

C. Deuterons

The deuteron beam current I_0 enters the absorber, is attenuated, and leaves with a reduced value, I. The following assumptions are made in the interpretation of the deuteron attenuation data:

* This work was performed under the auspices of the U. S. Atomic Energy Commission.
† California Research and Development Company, Livermore, California.
[1] Fernbach, Serber, and Taylor, Phys. Rev. **75**, 1352 (1949).
[2] R. Serber, Phys. Rev. **72**, 1008 (1947).
[3] J. DeJuren and N. Knable, Phys. Rev. **77**, 606 (1950).
[4] J. DeJuren, Phys. Rev. **80**, 27 (1950).
[5] W. P. Ball, thesis, University of California Report UCRL-1938 (unpublished).
[6] Bratenahl, Fernbach, Hildebrand, Leith, Moyer, de Juren, and Knable, Phys. Rev. **77**, 597 (1950).
[7] A. J. Kirschbaum, thesis, University of California Report UCRL-1967 (unpublished).
[8] F. F. Chen (private communication).
[9] Aron, Hoffman, and Williams, Atomic Energy Commission Report AECU-663 (unpublished).

1. All cross sections are assumed to be independent of energy in the region between 20 and 200 Mev.

2. The charged secondary particles are protons produced by the stripping of the deuterons.

3. The number of secondary charged particles other than stripped protons is negligible for the high-Z elements.

The current I for a high-Z element is given by

$$I=I_0e^{-\sigma_2 t}+\int_{t-\tau_1}^{t} I_0e^{-\sigma_2 x}\sigma_{2sp}e^{-\sigma_{1p}(t-x)}dx, \quad (1)$$

where t= the thickness of the attenuator, x= the distance traveled by a deuteron in the attenuator before suffering an inelastic collision, and $t-\tau_1$= the maximum depth in the attenuator from which secondary protons can escape. The most probable value of the kinetic energy $\langle T_p\rangle$ of the stripped proton is obtained by assuming that the proton has half the energy of the deuteron at the instant of stripping, plus the electrostatic energy gained by the proton due to the Coulomb barrier, minus half the binding energy ϵ_d of the deuteron

$$\langle T_p\rangle=\frac{1}{2}\left(T_d-\frac{Ze^2}{r'}\right)+\frac{Ze^2}{r'}-\frac{\epsilon_d}{2}=\frac{1}{2}\left(T_d+\frac{Ze^2}{r'}-\epsilon_d\right), \quad (2)$$

where r' is the distance between the center of the target nucleus and the incident particle; $\tau_1=t$ for $t<R_1(\langle T_p\rangle)$; and $\tau_1=R_2(T_d)-t$ for $t>R_1(\langle T_p\rangle)$, where $R_1(\langle T_p\rangle)$ and $R_2(T_d)$ are the mean ranges of the proton and deuteron of energies $\langle T_p\rangle$ and T_d, respectively, in the absorber.

Integrating Eq. (1) yields

$$I=I_0e^{-\sigma_2 t}\left[1+\frac{\sigma_{2sp}}{\sigma_1-\sigma_2}(1-e^{-(\sigma_1-\sigma_2)\tau_1})\right]. \quad (3)$$

If one defines Δ_d as the number of deuterons affected per unit thickness of absorber by inelastic collisions of the incident number of deuterons N_d, one may write $\Delta_d=\sigma_2 N_d$. Since each deuteron contains one proton, the number of affected protons is $\Delta_p=\sigma_2 N_d=\sigma_2 N_p$. The number of protons Δ_p' being attenuated is $\Delta_p'=\sigma_{1p}N_p=\sigma_{1p}N_d$, if it is assumed that the coupled proton acts as a free particle because of its weak binding. Therefore the total number of stripped protons Δ_{2sp} leaving the absorber becomes

$$\Delta_{2sp}=(\Delta_p-\Delta_p')=\sigma_{2sp}N_d. \quad (4)$$

Solving for an effective stripping cross section, one obtains

$$\sigma_{2sp}=\sigma_2-\sigma_{1p}. \quad (5)$$

Substituting in Eq. (3), we have

$$I=I_0\exp(-\sigma_2 t+\sigma_{2sp}\tau_1).$$

Therefore,

$$I=I_0e^{-\sigma_1 t} \quad \text{for} \quad t<R_1(\langle T_p\rangle), \quad (6a)$$

and

$$I=I_0\exp-(\sigma_2+\sigma_{2sp})t+\sigma_{2sp}R_2(T_d)$$
$$=I_0'\exp-(\sigma_2+\sigma_{2sp})t \quad \text{for} \quad t>R_1(\langle T_p\rangle). \quad (6b)$$

Thus, for high-Z elements, if the above assumptions are correct, a semilogarithmic plot of I/I_0 *vs* t should give an integral range curve composed of two straight-line segments with the change in slope at $t=R_1(\langle T_p\rangle)$.[10]

For the lower-Z elements, assumption (3) no longer holds. Consequently, interpretation of the integral range curves becomes difficult because of the large number of secondary knock-on charged particles. In order to minimize this effect, the following technique was employed (see Fig. 1). The integral range curve for uranium was first obtained. The uranium was then replaced by another element Z_i whose fixed thickness t_i (usually about half a range) reduced the incident beam energy from T_0 to T. Increments of uranium absorbers were then added between the absorber Z_i and the detector to obtain a series of integral range curves for different Z_i+U combinations. Many of the secondaries produced in the so-called primary absorber were then effectively prevented from being detected by the presence of the secondary uranium attenuator. For absorber thicknesses approximately $\frac{3}{4}$ the range of the incident deuteron no protons stripped in the absorber Z_i would be detected.

The number of deuterons leaving absorber Z_i is $I_i'=I_0e^{-\sigma_i t_i}$, and the number leaving the uranium is $I_i=I_0\exp(-\sigma_i t_i-\sigma_U t_U)$, where t_i and t_U are the respective thicknesses of the primary Z_i and secondary U attenuators, and σ_i is the total deuteron attenuation cross section for the ith element. A comparison of the value of the relative current I_i/I_0 at the end of the integral range curve of the Z_i+U combination with that of the total uranium relative current I_U/I_0 allows one to determine σ_i in terms of σ_U. For a complete range thickness R_U of uranium (aside from the usual range straggling), the number of deuterons left unattenuated is $I_U=I_0\exp(-\sigma_U R_U)$. Therefore at the ends

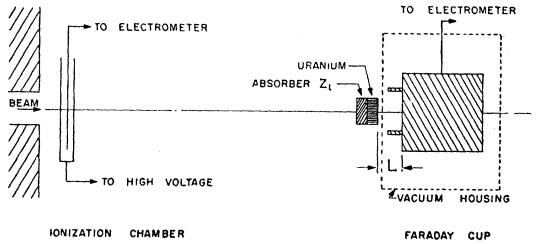

FIG. 1. Schematic diagram of experimental arrangement.

[10] An experiment by W. J. Knox at this laboratory first showed the tendency for the deuteron attenuation curve to fall on two straight lines with a break at the point $t=0.5R_2$. Only limits on the cross sections were determined because of the preliminary nature of his work.

of the ranges of the two curves, one can write the ratio,

$$\frac{I_i/I_0}{I_U/I_U}=\frac{\exp(-\sigma_i t_i)}{\exp\{-\sigma_U(R_U-T_U)\}}. \tag{7}$$

In the above equation, t_i and t_U are known experimental parameters, and I_i/I_0, I_U/I_0, and R_U are directly observable; therefore, one can easily solve for σ_i as a function of σ_U.

D. Protons

There appears to be no simple mechanism by which one can describe the production of secondary charged particles when high-energy protons traverse an absorber. The presence of such secondaries and/or a variation in the inelastic cross section with energy will introduce curvature into the integral range curves. Unlike the case for deuterons, there seems to be no basis one can use to test which of these two effects predominates. Thus the inelastic proton cross sections calculated from the integral range curves are subject to greater uncertainties than the deuteron cross sections.

The main purpose in measuring the proton inelastic cross sections was to test the agreement between the present method and that of Kirschbaum and Hicks.[7] To do this it is sufficient to measure an average cross section by assuming that a negligible number of secondary charged particles leaves the absorber for thicknesses nearly the range of the protons. Then the ratio I/I_0 for $t=R_1$ is given by

$$I/I_0=e^{-\sigma_1 R_1}, \tag{8}$$

which permits the calculation of σ_1, an average inelastic cross section.

The cross sections for various elements may be measured just as for deuterons, with Z_i+U absorbers, since there are essentially no secondary charged particles for $t_i+T_U\sim R_1$.

E. He^3 Particles

When a He^3 particle suffers an inelastic collision it is very likely to break up into its component nucleons, some of which are coupled to form deuterons.[11] Since the present experiment detects only the charged secondaries, it is sufficient to consider the stripped protons and deuterons. If the component nucleons of the He^3 particle are assumed to act as free particles because of their weak binding, then an argument exactly paralleling that given in Sec. IIC shows that

$$\sigma_{3sp}=2(\sigma_3-\sigma_{1p}), \tag{9}$$

where σ_{3sp} is the cross section for producing one stripped proton and σ_3 is the inelastic cross section for He^3 particles. The factor of 2 arises from the fact that the He^3 nucleus contains 2 protons. The most probable values of the kinetic energies of the stripped particles, neglecting small binding energy effects, may be expressed as

$$\langle T_p\rangle=\tfrac{1}{3}T_{He^3}+\tfrac{1}{3}Ze^2/r', \tag{10a}$$

$$\langle T_d\rangle=\tfrac{2}{3}T_{He^3}-\tfrac{1}{3}Ze^2/r'. \tag{10b}$$

If it is assumed that all secondary particles are produced with these energies, and the Coulomb energies are neglected, then the stripped protons produced will have a range 4/3 the residual range of the He^3 particles, whereas the stripped deuterons will have a range 8/3 the residual range of the He^3 particle. These secondary particles can be easily accounted for in calculating the inelastic cross sections from the integral range curves.

An analytic expression for the current as a function of absorber thickness ($0<t<8/3R_{3He^3}$) can be derived by using the techniques and results of Sec. IIC.[12]

F. Alpha Particles

Since the alpha particle is much more tightly bound than either the deuteron or the He^3 particle, an application of the previous method of calculating the current as a function of absorber thickness is not likely to prove fruitful.

If protons are "stripped" from an alpha particle during an inelastic collision, their residual range should be equal to the residual range of the alpha particle; because of the expected energy distribution of such stripped protons, their presence should tend to broaden the end of the integral range curve.

In spite of these difficulties the average inelastic cross section σ_4 may be determined from the discontinuity in beam current at the end of the alpha-particle range.

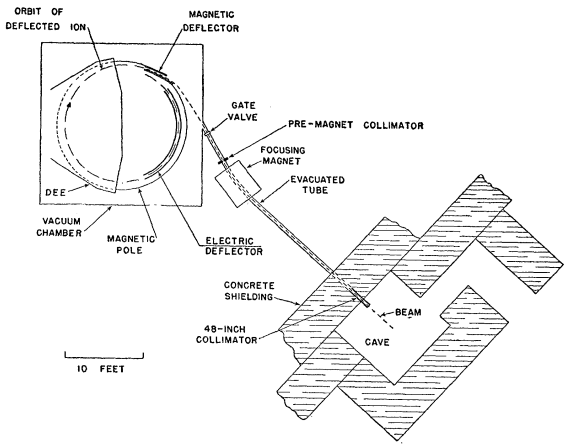

FIG. 2. Schematic diagram of the cyclotron, deflected beam path, and shielded enclosure.

[11] J. Ise *et al.*, University of California Report UCRL-2319 2nd Rev., Rev. Sci. Instr. **25**, 437 (1954).

[12] W. Birnbaum *et al.*, California Research and Development Company Report LRL-85 (unpublished) gives a more detailed report of this experiment.

III. EXPERIMENTAL METHOD

A. Procedure

The high-energy charged particles were electrically and magnetically deflected out of their circular orbits in the 184-inch cyclotron, and passed through a pre-magnet collimator, a focusing magnet, and a 48-inch collimator into the external experimental area. A plan view is shown in Fig. 2. The particles in the various deflected beams are essentially monoenergetic with probable energy spreads about their respective means of less than 1 percent.

The beams were monitored externally by a parallel-plate ionization chamber filled with helium to a pressure of 75 cm. For the beam levels employed in the present study, the chamber showed negligible recombination effects over a wide region of collection voltages (500–2500 volts). Figure 1 is a schematic diagram of the experimental apparatus. After passing through the monitor, the beam impinged upon the attenuating material. That portion of the beam which traversed the absorber was collected in a Faraday cup. The operating characteristics of the cup and the details of its behavior have been discussed previously by Aamodt *et al.*[13]

The charges collected by the monitor and the Faraday cup were placed on low leakage condensers connected to the inputs of integrating electrometers. The electrometer was of the 100 percent inverse feedback type; the electrometer signal was measured and recorded on a Leeds and Northrup Speedomax which automatically calibrated itself against a standard cell at frequent intervals. Since only the ratios of voltages entered into the final calculations, absolute calibration of the electrometers with their associated condensers and recorders was unnecessary. The procedure followed in the experiment was then to measure the ratio of the charges I and I_0 collected by the Faraday cup and ionization chamber, respectively, as a function of absorber thickness.

B. Scattering Corrections

For thick absorbers, the elastic scattering of the emergent unattenuated particles may be large enough to cause a decrease in the charge collected by the cup. This tends to give an apparent value for the inelastic cross section which is too high. To correct for this effect for incident deuterons and protons, the distance L (see Fig. 1) between the absorber and the Faraday cup was varied. This allowed an extrapolation of the ratio I/I_0 to the point where $L=0$. The corrections due to multiple Coulomb scattering were determined analytically by a graphical integration method.[14] Figure 3 shows the excellent agreement between the experimental points and the analytical curves for deuterons incident on two typical absorber thicknesses (carbon plus uranium, and uranium alone). It is to be noted that the scattering corrections are essentially negligible because of the large diameter of the Faraday cup. These small corrections as calculated by the graphical method were applied for absorber thicknesses up to 98 percent of the full range of the incident particle. Beyond that point, the magnitude of the scattering correction increases quite rapidly, introducing large uncertainties in its determination; the corrections were applied for $t/R>0.98$ by extrapolation, but this was done only to determine the mean range. (The cross section is insensitive to the precise location of the mean range point.) As will be discussed below, exact interpretation of the experimental points beyond 95 percent of the range was not attempted.

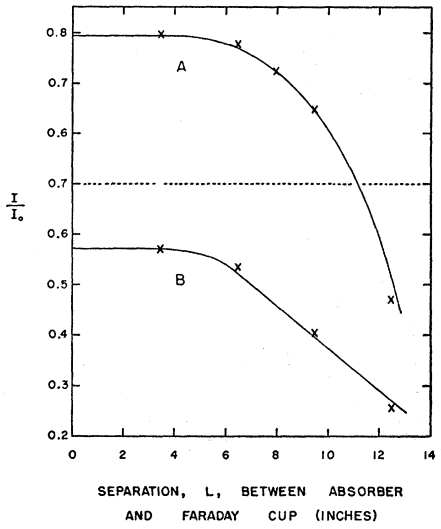

FIG. 3. Observed and calculated multiple scattering effect for 190-Mev deuterons. A. 28.0 g/cm² uranium ($t/R_2=0.88$). B. 6.526 g/cm² plus 17.20 g/cm² uranium ($t_U/R_{2U}'=0.96$). Crosses are the observed points.

For the low-Z elements, the agreement between the experimental points and the calculated scattering curve was not satisfactory. For 190-Mev deuterons incident on carbon, an attenuator 0.95 of a range thick showed a current loss of 10 percent when the separation L was increased from 3.5 to 12.5 in. A calculation predicted no drop in I/I_0 due to multiple scattering. The observed effect is believed to be caused by the relatively large number of charged secondary particles present in the beam of attenuated deuterons for low-Z absorbers. Since the experimental curve showed such a gentle fall, and since the calculated curves agreed with the experimental points for high-Z absorbers, the calculated corrections are used for the low-Z absorbers instead of attempting to determine an empirical correction. The calculated corrections to I/I_0 for beryllium and carbon were all zero for $t/R<0.98$.

For the Z_i+U combinations, where $Z_i\leq 29$, it was assumed that a negligible amount of Coulomb scattering

[13] R. L. Aamodt *et al.*, University of California Report UCRL-1400 (unpublished).

[14] W. C. Dickinson and D. C. Dodder, Los Alamos Report LA-1182 (unpublished).

occurred in the primary Z_i absorber, and corrections were then applied to the secondary uranium absorber. On the other hand, for the high Z_i+U combinations (Pb, Bi, and Ta), scattering corrections to the relative current were calculated assuming the combination to consist entirely of its equivalent thickness in uranium.

Scattering corrections were not calculated for the He^3 and He^4 beams for reasons to be discussed in Sec. IV.

The elastic scattering also tends to increase the effective thickness of the attenuator because the incident particles no longer travel in straight-line paths. To correct for this a second order path was assumed. The root-mean-square deviations perpendicular to the initial direction of the incoming beam were first calculated as a function of absorber thickness.[15] The parabolic path was then integrated to find the length t_c:

$$t_c = t_0[1+(2/9)\langle\theta^2\rangle],$$

where t_0 is the true thickness of the absorber, and t_c may be considered the effective thickness traversed by the incident particle; $\langle\theta^2\rangle$ is the mean square scattering angle for the thickness t_0. Since the corrections were small, the choice of the path was unimportant.

The number of very large-angle single-scattering events are considered to be negligible as is borne out by the excellent agreement between the experimental points and the multiple Coulomb scattering theory. This is especially true for the case of the deuteron where the associated small impact parameters required for large-angle scattering would probably cause the deuteron to break up into its component nucleons.

C. Range Straggling and Collimation

The shape of the integral range curve near its end is influenced by at least six effects: (1) range straggling, (2) small energy-transfer inelastic events, (3) scattering in the collimator, (4) energy distribution of the incident beam, (5) variation of cross section with energy, and (6) multiple scattering. The last has been discussed in the previous section. The result of these effects is to introduce a rounding off of the end of the curve. The variation of cross section with energy cannot be treated

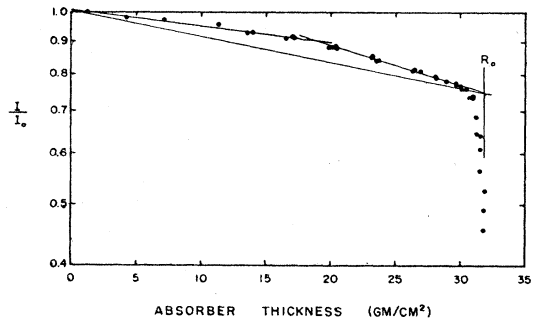

FIG. 4. Integral range curve for 190-Mev deuterons incident on uranium. The straight lines were fitted by least squares.

[15] B. Rossi and K. Greisen, Revs. Modern Phys. **13**, 240 (1941).

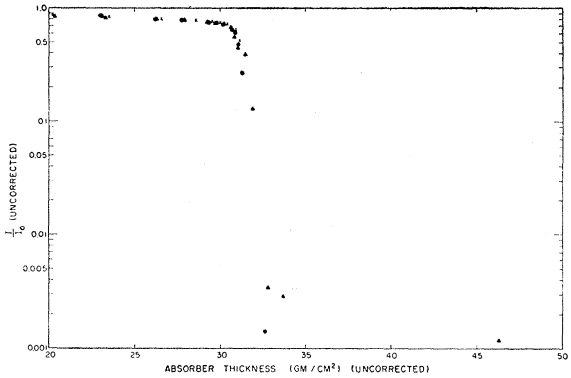

FIG. 5. Integral range curve for 190-Mev deuterons incident on uranium. Results of three runs are shown.

in this experiment and is felt to be a minor consideration in the energy regions with which we are concerned.

The mean range is taken as the point where energy losses due to ionization alone would reduce the current of particles to half its initial value; nuclear attenuation, etc., must be taken into account when the true current is measured. The mean range so defined is the center of an essentially Gaussian distribution whose width is a measure of the range straggling. Thus such straggling should result in rounding off the integral range curve. For 190-Mev deuterons and 340-Mev protons the half-width at half-maximum of the straggling curve is about 1 percent of the range.[16] The range straggling has been neglected in all the integral range curves, since points within 2 percent of the end of the range were not used.

If a particle undergoes an inelastic nuclear event in which it loses a very small amount of energy, then its final range will be only slightly shorter than its original range. Such particles would then stop near the end of the integral range curve and cause a rounding superimposed on the other effects, mainly range straggling and multiple scattering. After corrections for multiple scattering have been applied, the extent to which range straggling can be detected imposes a limit on the energy loss a particle must suffer to be counted as having had an inelastic event. Thus range straggling is the basis for the definitions of inelastic events for this experiment as given in Sec. II.

Scattering of the beam by the 48-inch collimator was reduced by adjusting the premagnet collimators; the energy selection of the focusing magnet prevented deuterons with degraded energies from passing through the 48-inch collimator. Under these conditions points were reproduced for different runs to within one percent for $t/R<0.95$.

Only points for $t/R<0.95$ were used in the final calculations. This procedure was followed as a precaution against uncertainties in I/I_0 near the end of the range.

[16] E. Segrè, *Experimental Nuclear Physics* (John Wiley and Sons, Inc., New York, 1953), Vol. 1.

The points for $0.95<t/R<0.98$ showed a tendency to fall below the straight line through the other points, but the discrepancies were not significant and were less than 4 percent for all cases.

IV. ANALYSIS OF DATA

A. Deuterons

1. Uranium

The experimental attenuation curves obtained for 190-Mev deuterons incident upon uranium (Fig. 4) show the characteristics discussed in Sec. IIC. Two straight lines were fitted by the method of least squares to the experimental points for $0<t<15$ g/cm^2 and $20<t<30$ g/cm^2, respectively, and extended until they intersected. The point of intersection at $t=0.57R_2$ ($t=18.2\pm0.7$ g/cm^2, $R_2(T_d)=31.8$ g/cm^2) allows one to calculate $T_{p\,\max}=103\pm2$ Mev. Substitution in Eq. (2) yields a value for the Coulomb barrier for uranium of 18 ± 4 Mev. If stripping is assumed to occur only at the edge of the nucleus, and if the charge is concentrated at the center, then the radius of the uranium nucleus is 7.3×10^{-13} cm, and $a_0=(1.2\pm0.3)\times10^{-13}$ cm. If, instead, stripping is assumed to occur throughout the volume, then the radius is 11×10^{-13} cm, and $a_0=(1.8\pm0.4)\times10^{-13}$ cm.

The straight-line fit applied to the latter half of the range is then extended to the end of the range. The inelastic deuteron cross section for an average deuteron energy of 120 Mev is determined from the slope of the straight line drawn from $t=0$ to $t=R_2$. These two points were chosen, since at $t=0$ no secondary particles have yet been produced, while at $t\geqq R_2$ the number of secondaries present is negligible as shown by Fig. 5. This gives a value for σ_2 of 3.81 ± 0.06 barns. The errors quoted above are statistical standard errors.

TABLE I. Inelastic cross sections for high-energy particles.

A. Neutrons

	84 Mev[a] (upper limits)	95 Mev[b] (lower limits)	270 Mev[c] (lower limits)	300 Mev[d]
Carbon	...	0.222±0.009	0.145±0.006	0.203±0.033
Aluminum	0.50±0.05	0.418±0.017	...	0.390±0.023
Copper	0.91±0.05	0.782±0.013	0.573±0.024	0.755±0.033
Lead	1.85±0.18	1.75 ±0.05	1.42 ±0.06	1.72 ±0.08

B. Protons (10 percent errors)

	305 Mev[e]	240 Mev[e]	185 Mev[e]	290 Mev	870 Mev[f]
Beryllium	0.151	0.169	0.172	...	0.171
Carbon	0.187	0.202	0.204	0.199	0.222
Aluminum	0.334	0.383	0.408	0.416	0.394
Copper	0.608	0.667	0.746	0.717	0.708
Lead	1.48	1.57	1.55	...	1.62
Uranium	1.60	1.77	1.90	1.85 2.03 (230 Mev)	

C. Deuterons, He^3, and alpha particles

	160-Mev H^2	315-Mev He^3	240-Mev He^4
Beryllium	0.512±0.025	...	...
Carbon	0.667±0.033	0.59±0.10	0.64±0.10
Aluminum	0.996±0.050	0.91±0.15	...
Copper	1.76 ±0.17	1.8 ±0.3	1.8 ±0.3
Tantalum	3.13 ±0.30	3.5 ±0.5	3.6 ±0.5
Lead	3.44 ±0.17	...	...
Bismuth	3.55 ±0.18	...	...
Uranium	3.81 ±0.15	4.4 ±0.7	...

[a] See reference 6.
[b] See reference 3.
[c] See reference 4.
[d] See reference 5.
[e] See reference 7.
[f] See reference 8.

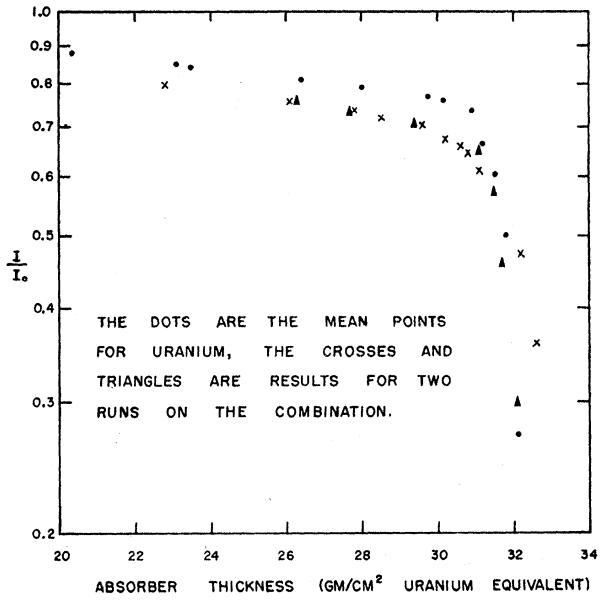

FIG. 6. Apparent attenuation of 190-Mev deuterons incident on carbon backed by uranium compared with the integral range curve for uranium.

The measurement of σ_1 for protons in uranium from the slope of the first part of the integral range curve [Eq. (6a)] is consistent with the proton attenuation work described below, and with the independent experiment of Kirschbaum and Hicks.[7] The slope $\sigma_1-2\sigma_2$ of the other straight-line segment [Eqs. (6b), (5)] gives another measurement of the deuteron inelastic cross section: $\sigma_2=3.95\pm0.12$ barns. The excellent agreement obtained from these different measurements of σ_2 and σ_1 indicates that the number of charged secondary particles other than stripped protons must be quite low.

2. U+Z_i Combinations

The C+U integral range curve is compared directly with the uranium curve in Fig. 6. The relative current $(I/I_0)_{C+U}$ has been plotted as a function of the absorber thickness in g/cm^2 uranium equivalent. The conversion to equivalent uranium thickness was made from the range R_2 in uranium and the range R_2' in Z_i+U. As above, a straight line is fitted to the latter half of the experimental data up to $0.95R_2$ and then extrapolated to the mean range point. Table I gives the inelastic cross sections for all the absorbers used. The standard errors shown in Table I for the deuteron cross sections are not statistical errors, but have been increased to take account of possible systematic effects by doubling the statistical error for the uranium cross section.

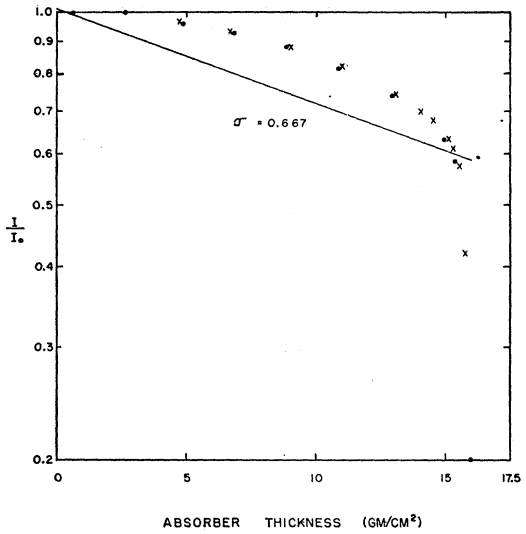

FIG. 7. Integral range curve for 190-Mev deuterons incident on carbon. The straight line is drawn for the cross section determined by C+U attenuation. Two runs are shown.

3. Carbon

The curve for C is presented in Fig. 7. As discussed in Sec. IIC, the presence of a large number of charged secondaries causes this integral range curve to show a continuously changing slope. Hence, the theory which is applicable for uranium is no longer suitable. Only rough estimates of σ_2 can be made from this curve since the location of the mean range points is uncertain. The slope of the straight line superimposed on the experimental data represents the inelastic cross section calculated from the U+Z_i combination method. The straight line is not inconsistent with the experimental points, and illustrates the effectiveness of the combination method in reducing uncertainties arising from the secondaries.

B. Protons

The inelastic cross sections for high energy protons were determined essentially as in Part A. The integral range curve for uranium, Fig. 8, shows a smoothly varying slope and there appears to be no simple theory to explain the shape. Instead, the shape was assumed to result from a combination of the variation of the cross section with energy and the detection of secondary particles. Since there should be essentially no secondary particles for $t \geqq R_1$, the average cross section was determined by a straight line joining $\log(I/I_0)$ at $t=0$ and $t=R_2$. The mean energy was 230 Mev for this case.

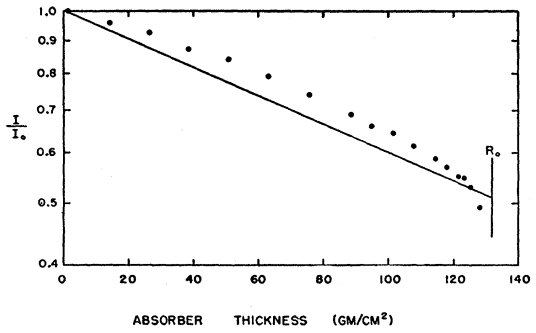

FIG. 8. Integral range curve for 340-Mev protons incident on uranium. The straight line is drawn for the cross section determined by extending the end of the curve to R_0 (mean range point). Corrections for multiple scattering were applied.

The attenuation cross section for protons in carbon, aluminum and copper were determined by Z_i+U combinations as in Part A for deuterons. A typical attenuation curve for carbon plus uranium is shown in Fig. 9. The mean energy of protons in the Z_i primary attenuator was 290 Mev, so the inelastic cross section for uranium had to be extrapolated to 290 Mev. This was done by using the curve drawn through plots of $\log\sigma_1$ *vs* energy shown in Fig. 10.

The proton inelastic cross sections determined in this experiment are listed with those determined by Kirschbaum and Hicks[7] in Table I. The present values tend to be systematically higher; since the effect of secondary particles in the attenuated proton beam would be to decrease the measured cross section, a possible explanation is in the difference between the definition of inelastic events in the two experiments. Kirschbaum and Hicks call an event inelastic if the proton loses 10 percent of its incident energy (34 Mev), whereas it is believed that this experiment measures an event as inelastic if the energy loss is 15 Mev. The systematic difference between the two sets of measurements may be a measure of the number of inelastic events in which the proton loses between 34 and 15 Mev of energy. The present measurements may be low if there are many inelastic events with energy loss between 0 and 15 Mev.

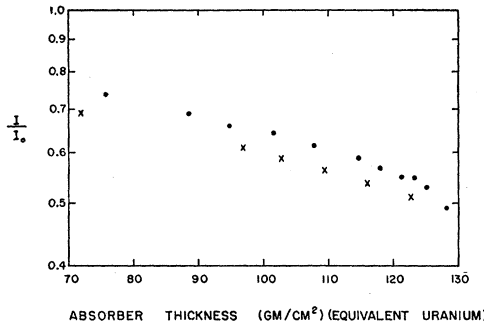

FIG. 9. Apparent attenuation of 340-Mev protons incident on carbon backed by uranium compared with the integral range curve for uranium. The dots are for uranium, the crosses for carbon backed by uranium.

C. He^3 Particles

The secondary particles formed when an incident He^3 particle breaks up have residual ranges greater than the residual range of the He^3 particle (Sec. IIE). Thus

to determine the inelastic cross sections σ_3, the integral range curve must be measured for each element individually instead of using the Z_i+U combination technique. A typical integral range curve is shown in Fig. 11.

Although the experimental points do not allow sharp differentiation between the secondary protons and deuterons, it appears qualitatively from the residual range analysis that a significant fraction of the secondaries are deuterons.

The cross section is determined by subtracting I/I_0 for $t=R_{3\mathrm{He}}+\delta$ from I/I_0 for $t=R_{3\mathrm{He}}-\delta$ (δ is a small increment of absorber around the mean range point)

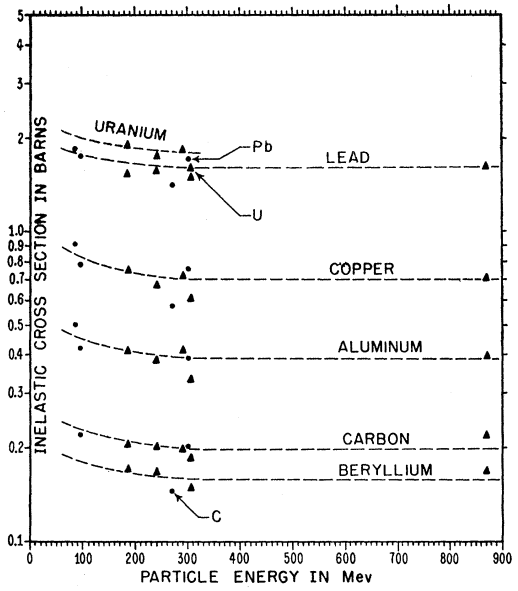

FIG. 10. Inelastic cross sections for high energy protons (triangles) and neutrons (dots) plotted as a function of the energy. The lines were drawn to give smoothed values; the slope of the line for uranium was drawn equal to that for lead; the slopes of the lines for carbon and beryllium, equal to that for aluminum. References for the points are given in Table I.

and assuming the cross section to be independent of the energy. The cross sections σ_3 are listed in Table I. No scattering corrections were made since the subtraction removes their effect. The effect of multiple scattering on the range is much smaller than the uncertainty in the location of the mean range point, and hence can be neglected.

It is assumed that a 15 percent standard error is a conservative estimate of the uncertainties in the measured cross sections for all elements.

D. Alpha Particles

To measure the inelastic cross section σ_4 for alpha particles, the same technique was used as for He^3 particles. The number of secondary particles is much lower as shown in a typical integral range curve, Fig. 12.

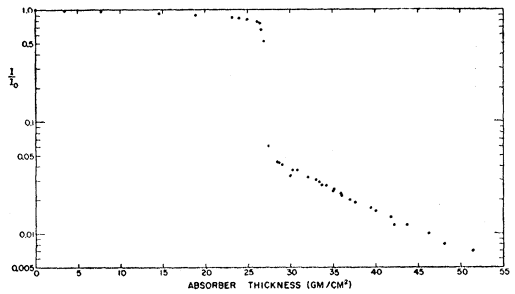

FIG. 11. Integral range curve for 490-Mev He^3 particles incident on tantalum.

The cross sections σ_4 are included in Table I. The standard errors in these cross sections are again assumed to be 15 percent for all elements.

The secondary protons are expected to have an average range approximately equal to the range of the alpha particles. The momentum distribution of the protons in the He^4 nucleus should be reflected in a broad distribution of the proton ranges. The absence of secondary protons is shown by the sharp fall-off of the integral range curves at $t=R_4$ and the low current for $t>R_4$. If such protons were present, the cross sections measured would be too low.

V. INTERPRETATION OF THE DATA

A. Deuteron Stripping Cross Sections

As shown in Sec. IIC, the quantity $\sigma_{2sp}=\sigma_2-\sigma_{1p}$ may be taken as a cross section for stripping a proton from an incident deuteron. σ_{1p} for a proton of half the mean energy of the deuterons should be used, and in this energy region $\sigma_{1p}\approx\sigma_{1n}$ so that the inelastic cross sections for 80-Mev neutrons from Fig. 10 may be used. Table II gives the difference $\sigma_2-\sigma_{1n}$ for elements whose cross sections are known, and these are plotted against the mass number A in Fig. 13. The stripping cross section varies approximately as $A^{\frac{1}{2}}$ in disagreement with the variation expected if the stripping process were a pure edge ($A^{\frac{1}{3}}$) interaction. The effects of

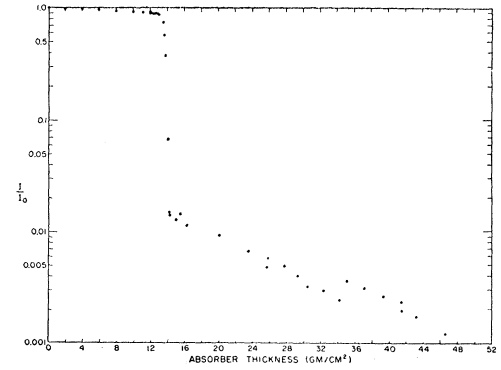

FIG. 12. Integral range curve for 380-Mev alpha particles incident on tantalum.

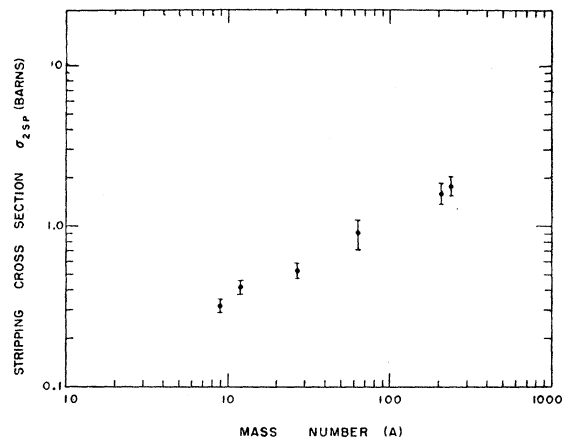

FIG. 13. The cross section for producing a stripped proton from 160-Mev deuterons ($\sigma_2-\sigma_{1p}$) plotted as a function of the mass number A.

electric stripping are less than the standard errors of the cross sections.[17]

These stripping cross sections, inferred from a measurement of the deuteron attenuation, are in reasonable agreement with those inferred from a measurement of the angular distribution of the secondary protons at relatively large angles.[18] The present method avoids the necessity of choosing a specific model for the stripping process.

The relative stripping cross sections measured by W. J. Knox[19] agree with this variation with A.

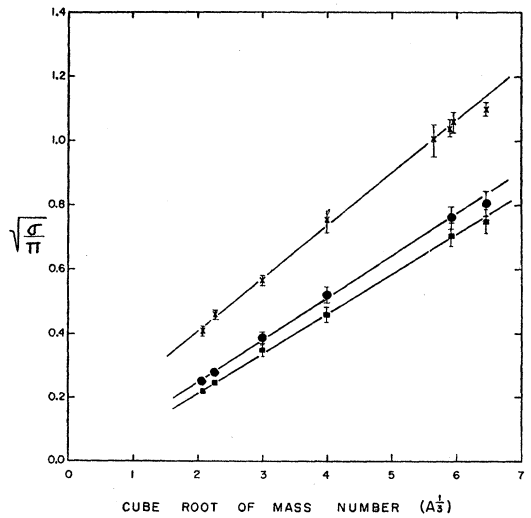

FIG. 14. Plot of $(\sigma/\pi)^{\frac{1}{2}}$ *vs* $A^{\frac{1}{3}}$ for 80-Mev and 300-Mev neutrons, and 160-Mev deuterons.

[17] S. M. Dancoff, Phys. Rev. **72**, 1017 (1947).

[18] L. Schecter *et al.*, Phys. Rev. **90**, 633 (1953); L. Schecter and W. Heckrotte, University of California Radiation Laboratory Report UCRL-2516 [Phys. Rev. **94**, 1086 (1954)].

[19] W. J. Knox, Phys. Rev. **81**, 687 (1951).

B. Inelastic Cross Sections

Figures 14, 15, and 16 clearly show that the inelastic cross section for a bombarding particle of n nucleons can be written

$$\sigma_n=\pi(a_nA^{\frac{1}{3}}+r_n')^2. \tag{11}$$

The parameters a_n and r_n' were determined by the method of least squares and are listed in Table III. Equation (11) is open to certain interpretations. If one takes $r=a_nA^{\frac{1}{3}}$ as the radius of the nucleus, then r is a function of the bombarding particle. It appears to us that a more satisfying assumption is that r is independent of n, and that $r=a_0A^{\frac{1}{3}}$, where we write

$$a_n=a_0(1-\tau_n)^{\frac{1}{3}}. \tag{12}$$

In Eq. (12) τ_n is the nuclear transparency for a bombarding particle of n nucleons. If we then assume a similar expression for r_n' (r_n is associated with the size of the bombarding particle), Eq. (11) can be written

$$\sigma_n=\pi(a_0A^{\frac{1}{3}}+r_n)^2(1-\tau_n). \tag{13}$$

TABLE II. Cross section for producing stripped protons from 160-Mev deuterons.

Element	Inelastic cross section for 160-Mev deuterons, σ_2	Inelastic cross section for 80-Mev neutrons, σ_1 (see Fig. 10)	σ_{2sp} $(\sigma_2-\sigma_1)$
Beryllium	0.512±0.025	0.185±0.019	0.33±0.03
Carbon	0.667±0.033	0.237±0.024	0.43±0.04
Aluminum	0.996±0.050	0.465±0.047	0.53±0.05
Copper	1.76 ±0.17	0.85 ±0.09	0.91±0.19
Lead	3.44 ±0.17	1.81 ±0.18	1.63±0.25
Uranium	3.81 ±0.15	2.06 ±0.20	1.75±0.25

Note: The error in σ_1 was estimated as 10 percent for all elements.

The behavior exhibited by the inelastic cross sections is of value in determining the structure of the nucleus and its interactions with bombarding particles. We first consider how the optical model of the nucleus proposed by Fernbach, Serber, and Taylor[1] is affected by the present data. In their model they assume $a_0=1.4\times10^{-13}$ cm and a nuclear transparency τ which varies with A; these parameters were chosen to fit the total neutron cross sections. In Fig. 17 two curves calculated from the model with $a_0=1.35\times10^{-13}$ cm, $K=3.0\times10^{12}$ cm^{-1}, and $a_0=1.7\times10^{-13}$ cm, $K=1.0\times10^{12}$ cm^{-1} are shown together with the data from Fig. 10 for 80-Mev neutrons. The agreement with the first curve is satisfactory, since the systematic difference for the lighter elements could be due to a failure of the model. The figure clearly shows that the second curve cannot be considered satisfactory. The curves have a very straight portion for $2<A^{\frac{1}{3}}<6$ which is not changed for wide variations in a_0 or K. The slope of this portion is governed by the choice of a_0 and the position by the choice of K; the lines are insensitive to K for $\infty>K>10^{12}$ cm^{-1}, but begin to curve for

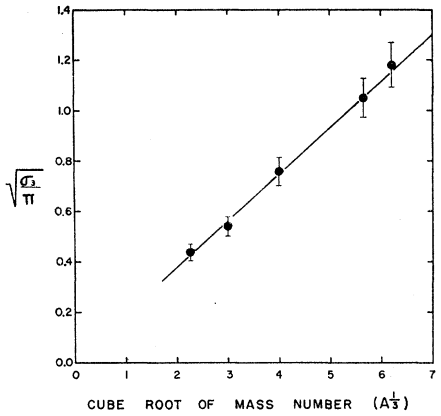

FIG. 15. Plot of $(\sigma_3/\pi)^{\frac{1}{2}}$ *vs* $A^{\frac{1}{3}}$ for 315-Mev He^3 particles.

$K<10^{12}$ cm^{-1}. An interesting feature is the negative intercept obtained by extrapolating the straight portions to $A^{\frac{1}{3}}=0$. Thus the optical model produces the important features shown by $\sqrt{\sigma_1}$ in Fig. 14: a straight line for $2<A^{\frac{1}{3}}<6$ with a negative intercept. It should be mentioned that the curve for $K=\infty$, $a_0=1.25\times10^{-13}$ cm (a straight line through zero), fits the data better than the curve shown.

The optical model of Fernbach *et al.* explains the variation of σ_1 with A in a satisfactory manner, but it is clear from the magnitudes of σ_2, σ_3, and σ_4 that the model in its present form cannot be entirely correct. Considering σ_2, it is apparent that the nucleus must extend to a radius of the order of $1.7\times10^{-13}A^{\frac{1}{3}}$ cm, and the magnitudes of σ_3 and σ_4 show that the larger radius is not peculiar to the deuteron. Independent evidence from the Coulomb scattering of alpha particles tends to confirm this conclusion.[20] The curve for $a_0=1.7\times10^{-13}$ cm in Fig. 17 indicates that the nucleus cannot be considered as a sphere of constant density.

Thus a simple square-well potential for a nucleus of constant density does not appear to be capable of explaining the present results in a consistent manner, but the agreement between σ_1 as observed and as calculated from the optical model leads one to believe that a potential not radically different from a square-well might be appropriate. A modified potential with a fringe extending to the outermost radius of the nucleus appears to be a reasonable assumption. The results for σ_2, σ_3, and σ_4 indicate that such a fringe should increase linearly with $A^{\frac{1}{3}}$.

TABLE III. Slopes and intercepts for straight-line fits of inelastic cross sections.

Particle	Mean energy (Mev)	Slope $\times10^{13}$ (cm)	Intercept $\times10^{13}$ (cm)
Neutron	80	1.37±0.07	−0.33±0.20
Neutron	300	1.26±0.06	−0.41±0.18
Deuteron	160	1.68±0.04	0.64±0.08
He^3	315	1.92±0.18	−0.12±0.61
Alpha	240	1.84±0.42	0.35±1.1

[20] G. W. Farwell and H. E. Wegner, Phys. Rev. **93**, 356 (1954).

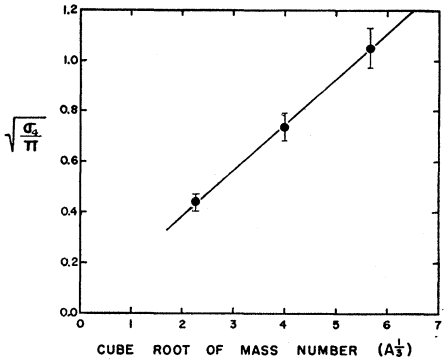

FIG. 16. Plot of $(\sigma_4/\pi)^{\frac{1}{2}}$ *vs* $A^{\frac{1}{3}}$ for 240-Mev alpha particles.

The assumption of constant density over the entire nucleus would probably need modification for such a potential, but the data do not permit determination of the form of the nuclear density distribution.

The nuclear transparency resulting from the optical model was based on a constant-density, spherical nucleus. It is interesting to consider a transparency which is an average over the entire nucleus including the fringe. It is assumed that the nucleus interacts with the individual nucleons in a bombarding particle, and that if τ is the transparency for a single-nucleon particle, then τ^2 is the transparency for a two-nucleon particle, etc. Equation (13) can then be written

$$a_n=\pi(a_0A^{\frac{1}{3}}+r_n)^2(1-\tau^n). \tag{14}$$

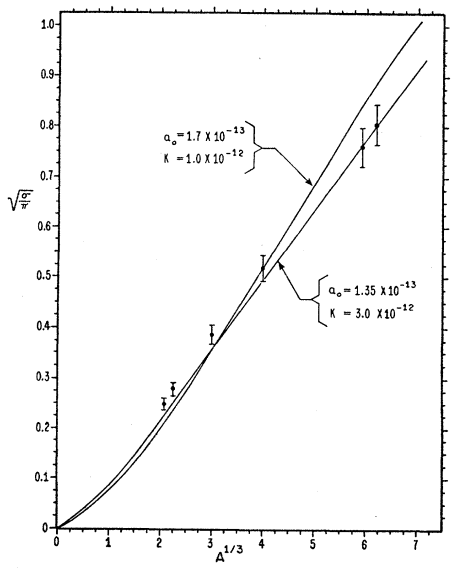

FIG. 17. Calculated (curves) and observed (dots) values of $(\sigma_1/\pi)^{\frac{1}{2}}$ for *vs* $A^{\frac{1}{3}}$ 80-Mev neutrons. K was chosen to fit curves to dots near $A^{\frac{1}{3}}=4$.

The parameters a_0 and τ, both assumed independent of A, as calculated by the method of least squares are

$$\tau=0.55\pm0.12, \quad a_0=2.0\pm0.3, \tag{15}$$

as obtained by using the data for σ_1, σ_2, and σ_3 only. The alpha particle data were not used since the binding energies of the particles reach a peak for He^4, and this system should not be expected to satisfy the independent nucleon assumptions to the same degree as the more loosely bound particles.

The transparency given in Eq. (15) is not strictly independent of A since the curves in Fig. 14 for σ_1 have negative intercepts, but the variation with A is not extreme. Equation (14) can be rewritten

$$(\sigma_n/\pi)^{\frac{1}{2}}=(a_nA^{\frac{1}{3}}+r_n)(1-\tau^n)^{\frac{1}{2}}. \tag{16}$$

The ratio

$$[1-\tau_n(A)]^{\frac{1}{2}}=(\sigma_n/\pi)^{\frac{1}{2}}/a_0A^{\frac{1}{3}}+r_n,$$

with $a_0=2.0\times10^{-13}$ cm, $r_1=0$, $r_2=0.75\times10^{-13}$ cm, $r_3=0$, is given in Table IV for $n=1$, 2, and 3.

The values calculated from $\tau=0.55\pm0.12$ are $(1-\tau)^{\frac{1}{2}}=0.67\pm0.08$, $(1-\tau^2)^{\frac{1}{2}}=0.84\pm0.07$, and $(1-\tau^3)^{\frac{1}{2}}=0.91\pm0.05$. The agreement shows that the assumption $\tau_n=\tau^n$ is not inconsistent with the data.

VI. SUMMARY AND CONCLUSIONS

The inelastic cross section for a particle of n nucleons bombarding a nucleus of mass number A can be accurately represented by the equation

$$\sigma_n=\pi(a_nA^{\frac{1}{3}}+r_n')^2, \tag{11}$$

where a_n and r_n' vary with n.

Although the data for σ_1 are explained satisfactorily by the optical model of Fernbach, Serber, and Taylor,[1] the data for σ_2, σ_3, and σ_4 require nuclear radii larger than their model will permit. If the nuclear potential is modified to include a fringe, the present data indicate that the fringe increases linearly with $A^{\frac{1}{3}}$.

Another expression which describes the cross sections with fewer parameters is

$$\sigma_n=\pi(a_0A^{\frac{1}{3}}+r_n)^2(1-\tau^n), \tag{14}$$

but no nuclear model is known which leads to this relation. The assumption of $\tau_n\neq0$ for $n>1$ introduces the idea of nuclear transparency for multinucleon particles as such. It may seem strange to assume that a loosely bound particle such as the deuteron can pass through the potential of the nucleus and emerge as a deuteron, since the phase changes between the component nucleons induced by the nuclear potential at first thought would seem to preclude the chance that the neutron and proton would emerge coupled to form a deuteron. The fact that deuteron and triton pickup[21] occur when the component nucleons have widely different initial relations of phase and momentum makes the idea of deuteron transparency plausible since in the present case the two nucleons start with the initial relations required for the formation of a deuteron.

Our results indicate a much larger extent for the nucleus than other recent experiments.[22,23] Fitch and Rainwater find $a_0=1.2\times10^{-13}$ cm from experiments with μ mesons and a high energy electron scattering experiment of Hofstadter *et al.* gives approximately $a_0=1.1\times10^{-13}$ cm. These two experiments of course do not measure the same part of the nucleus as our experiment; in particular, they measure the charge distribution and in any case would be insensitive to the nuclear fringe. The argument advanced that neutron scattering experiments measure the outer range of the nucleus is not consistent with our results. It may be that the recent model of the distribution of neutrons and protons in the nucleus proposed by Teller and Johnson[24] will explain the difference between the experiments, or it may be that a suitable choice of the shape of the nuclear potential in itself will be sufficient. As is shown by Heckrotte[25] in the following paper, even the choice of a crude nuclear potential which has the features of a fringe area seems to give better agreement between the different experiments than one would expect.

The stripping cross section derived from the present data varies approximately as $A^{\frac{1}{3}}$, which indicates that an interaction which varies as $A^{\frac{2}{3}}$ probably should be added to Serber's expression.

TABLE IV. Square root of the nuclear opacity as a function of $A^{\frac{1}{3}}$ for nuclear radii given by $2.0A^{\frac{1}{3}}\times10^{-13}$ cm.

$A^{\frac{1}{3}}$	Ratio for neutron cross sections $(1-\tau_1)^{\frac{1}{2}}$	Ratio for deuteron cross sections $(1-\tau_2)^{\frac{1}{2}}$	Ratio for He^3 cross sections $(1-\tau_3)^{\frac{1}{2}}$
2.03	0.60	0.82	...
2.26	0.62	0.87	0.96
3.00	0.64	0.83	0.90
3.99	0.65	0.86	0.95
5.92	0.64	0.82	0.93 ($A^{\frac{1}{3}}=5.65$)
6.20	0.65	0.84	0.95

VII. ACKNOWLEDGMENTS

The authors are happy to acknowledge the encouragement and assistance of Dr. C. M. Van Atta. We are indebted to Dr. Warren Heckrotte for stimulating discussions concerning the interpretation of the data, and to Mr. Donald Hicks, Dr. John Ise, Mr. Robert Main, and Dr. Robert Pyle for assistance in collecting the data and in maintaining the equipment. Finally, thanks are due to Mr. James Vale, members of the cyclotron crew, and the electrometer maintenance group of the University of California Radiation Laboratory.

[21] J. Hadley and H. York, Phys. Rev. **80**, 345 (1950).
[22] V. L. Fitch and J. Rainwater, Phys. Rev. **92**, 789 (1953).
[23] L. I. Schiff, Phys. Rev. **92**, 988 (1953).
[24] M. H. Johnson and E. Teller, Phys. Rev. **93**, 357 (1954).
[25] Warren Heckrotte, University of California Radiation Laboratory Report UCRL-2510, following paper [Phys. Rev. **95**, 1279 (1954)].